MNRAS **000**, 1–13 (2016) Preprint 8 September 2016 Compiled using MNRAS LATEX style file v3.0

Simultaneous Optical/X-ray study of GS 1354-64 (= BW Cir) during hard outburst: evidence for optical cyclo-synchrotron emission from hot accretion flow

Mayukh Pahari[1,2]*, Poshak Gandhi[2], P. A. Charles[2], M. M. Kotze[3], Diego Altamirano[2], Ranjeev Misra[1]

[1] *Inter-University Centre for Astronomy and Astrophysics, Pune, 411007, India*
[2] *School of Physics & Astronomy, University of Southampton, Highfield, Southampton SO17 1BJ, UK*
[3] *South African Astronomical Observatory, PO Box 9, Observatory 7935, South Africa*

8 September 2016

ABSTRACT

We present results from simultaneous optical (*SALT*) and X-ray (*Swift* and *INTEGRAL*) observations of GS 1354-64/BW Cir during the 2015 hard state outburst. During the rising phase, optical/X-ray time series show a strong anti-correlation with X-ray photons lagging optical. Optical and X-ray power spectra show potential quasi-periodic oscillations at $\sim$ 18 mHz with at least 99% confidence. The auto-correlation function of optical and X-ray lightcurve have equal widths and similar pattern upto 30 sec. Simultaneous fitting of *Swift*/XRT and *INTEGRAL* spectra in the range 0.5−1000.0 keV shows non-thermal, power-law dominated ($>$ 90%) spectra with a hard power-law index of 1.48 $\pm$ 0.03, inner disc temperature of 0.12 $\pm$ 0.01 keV and inner disc radius of $\sim$3000 km. All evidence is consistent with cyclo-synchrotron radiation being the major physical process for the origin of optical photons in a non-thermal, hot electron gas cloud which extends to $\sim$ 100 Schwarzschild radii, rather than outer disc X-ray reprocessing. With an increase in X-ray count rate by a factor of $\sim$2.5, the optical flux decreases and the apparent features in optical/X-ray correlation vanish. At the peak of the outburst, both optical and X-ray variability is dominated by their noise components and the inner disc temperature increases up to 0.49 keV.

Key words: accretion, accretion discs — black hole physics — X-rays: binaries — X-rays: individual: GS 1354−64

1 INTRODUCTION

In the field of accretion physics, substantial progress has been made in the last decade using correlated optical/X-ray studies which can connect inner accretion phenomena with outer accretion disc activity (van Paradijs & McClintock 1994; de Jong et al. 1996; Esin et al. 2000; Kanbach et al. 2001). Very recently it has been realized that to fully understand the accretion and radiation mechanism in the innermost part of the accretion disc (that emits mostly in X-rays), simultaneous, multi-wavelength observations are indispensable (Uttley & Casella 2014; Russell & Fender 2010). One reason is the large variation in the time-scales involved in different physical processes that are responsible for emission other than X-rays. The observed range of time-scales can vary from a few tens of milliseconds to a few hundreds of seconds (e.g., Gandhi et al. (2016) and references therein). With new observatories such as ASTROSAT that facilitate high time resolution studies, the field of correlated optical/X-ray studies will become information rich, leading us to a clearer understanding of accretion structure and evolution.

The origin of optical photons is thought to be driven by the reprocessing of the hot, energetic, inner disc photons from the outer cold disc (Shakura and Sunyaev 1973). In both cases, a rise in the X-ray flux will prompt a rise in the optical flux or vice versa depending upon which of the two events takes place first. Such phenomena lead to the detection of a strong, positive peak in the cross-correlation function (CCF) of the X-ray/Optical time series with some delay time, of the order of a few seconds to a few tens of seconds depending upon the size of the re-processor. Recent simultaneous optical/X-ray observations from different

* E-mail: mayukh@iucaa.in (MP)

black hole X-ray binaries show that there exists a strong anti-correlation between optical/X-rays in the hard state with X-ray photons lagging optical photons by a few seconds (Durant et al. 2008; Gandhi et al. 2008; Malzac et al. 2003; Kanbach et al. 2001). The observed anti-correlation is in sharp contrast with lagged positive correlation predicted by the reprocessing or fluctuation propagation of viscous dissipation mechanisms. Interestingly, not only in BHXBs, but also a few neutron star X-ray binaries like Sco X-1, Cyg X-2 also show anti-correlation between optical/X-ray simultaneous time-series (Durant et al. 2011).

Sometimes, along with the anti-correlation, a strong positive peak is observed in the CCF which complicates the interpretations of the origin of optical photons (e.g., Gandhi et al. (2008)). To interpret correlated optical/X-ray complex behaviour and the lag time scale which is of the order of fluctuation propagation time-scales (Kanbach et al. 2001), the X-ray photons are assumed to originate from the thermal Comptonization of the synchrotron radiation in an accretion disc corona (Merloni et al. 2000). Alternatively magnetized outflows connecting both X-ray and optical emission locations are proposed to explain optical/X-ray correlated behaviour. However, both models fail to explain the 'precognition dip', an anti-correlation prior to the strong lagged correlation, in the CCF. To explain this feature, a magnetic reservoir model has been proposed (Malzac et al. 2004). This model assumes that an intense magnetic field can be generated using dynamo action in the disc, therefore magnetic flux tubes (di Matteo et al. 1999) of different scale heights sandwiching the disc, can store enormous amounts of energy to feed both jet and corona in a self-consistent manner (Malzac et al. 2004). The observed optical/X-ray anti-correlation can be explained by this model along with some of the complex patterns in the CCF by assuming linear superposition of fluctuating shots. Later, this was improved by replacing linear superposition with non-linear coupling of shots (Uttley et al. 2005; Gandhi 2009). However, the origin of quasi-periodic oscillations (QPOs) with time-scales of milliseconds to tens of seconds in both optical (Motch et al. 1983; Durant et al. 2009; Gandhi et al. 2010) and UV (Hynes et al. 2003) bands is difficult to explain using the magnetic reservoir model.

During the low/hard state, defined as an accretion state in X-ray binaries dominated by flat powerlaw emission and strong band limited-noise in Fourier power spectra (Remillard & McClintock 2006), the inner part of the truncated disc is usually filled with a hot, relativistic electron plasma (Yuan & Narayan 2014) along with intense magnetic fields (Esin et al. 1997). The idea that such magnetized hot flow could be the birthplace of optical photons by means of electron-cyclotron emission, was introduced by Fabian et al. (1982) and successfully explained the fast variability observed from GX 339-4 (Motch et al. 1983), 20-sec X-ray QPOs and the observed X-ray/optical anti-correlation in the CCF. Using reasonable assumptions, it was noted that the 20-sec QPO time-scale corresponds to the in-fall time in the hot flow region (Fabian et al. 1982). One of the major predictions of the cyclo-synchrotron model is the detection of QPOs in both X-ray and optical with similar time-scales. According to the Lense-Thirring precession model (Stella & Vietri 1998; Ingram, Done & Fragile 2009), the generation of simultaneous optical and X-ray QPOs is possible within the hot flow due to precession of the inner hot flow. Despite many optical/X-ray correlated studies in several X-ray binaries with improved instrumentation (Kimura et al. 2016; Gandhi et al. 2016; Shahbaz et al. 2015), there exists no strong evidence against the cyclo-synchrotron origin of optical photons from the hot inner flow. Apparao (1984) shows that in the case of Cyg X-1, EUV photons produced by cyclotron emission can act as seed photons for high energy (> 10 keV) Comptonization. The optical emission is interpreted as reprocessed X-rays from the outer disc (Shakura and Sunyaev 1973) which is consistent with the fact that the observed optical flux is $\sim$ 1% of the high energy X-ray flux the (theoretically predicted range is 0.1−10%; Shakura and Sunyaev (1973)). The observed optical flux from GX 339-4, however, is higher than that estimated by the cyclotron process (Apparao 1984).

GS 1354-64 (= BW Cir) is a black hole X-ray transients that has a X-ray outbursts three times in 28 years. During its 1997 outburst, *RXTE* detected moderate flux ($\sim$ 30-40 mCrab) but interestingly, throughout the outburst, the source remained in the hard state. Since GS 1354-64 is close to the poorly located Cen X−2, a soft X-ray transient, discovered in 1967 with a peak X-ray flux of $\sim$ 8 Crab, it is likely they are the same source (Kitamoto et al. 1990). Using optical spectroscopy of GS 1354-64, Casares et al. (2009) presented dynamical evidence for a 7.9 ± 0.5 M⊙ BH. With $P_{orb} = 2.54$ days (Casares et al. 2009), the donor is a G0-5 III star (Casares et al. 2004) of mass 1.1 ± 0.1 M⊙ (from the rotational broadening of the companion's absorption spectrum). Interestingly, during quiescence, GS 1354-64 shows strong optical variability (Casares et al. 2009) with R filter falling by 4 magnitudes ($\sim$ 17 to $\sim$ 21) over a period of 14 years. Casares et al. (2009), subsequently constrained the source distance and disc inclination angle to be $\geqslant 25$ kpc and $\leqslant 79^{\circ}$ respectively.

The outburst of GS 1354-64 in 2015 was first reported by Miller et al. (2015a) when they detected a 0.5-10.0 keV X-ray flux 260 times higher than that in quiescence. *Swift*/XRT X-ray spectra on 10 June 2015 gave a power-law photon index of 1.5 ± 0.1 (Miller et al. 2015b). Using the SOAR Optical Imager (SOI) at Cerro Pachon, Chile, Corral-Santana et al. (2015) measured the g', r' and i' magnitudes to be $\sim$19.76, $\sim$18.49, $\sim$18.34 respectively on 10-11 June, 2015. The detailed evolution of the 2015 outburst in GS 1354-64 at optical, UV and X-ray bands has been presented by Koljonen et al. (2016). They find that the optical/UV emission is tightly correlated with the X-ray emission on time-scales of days.

In this work, we present simultaneous X-ray (*Swift*/XRT and *INTEGRAL*) and optical (*SALT*/BVIT) variability studies of GS 1354-64 during the 2015 X-ray outburst. We observe a strong anti-correlation between X-ray and optical on time-scales of < 10 sec and harder X-rays show stronger anti-correlation with optical than soft X-rays. We perform simultaneous broadband spectral analysis in the energy range 0.5-1000.0 keV and show that all spectral and timing signatures strongly suggest that cyclo-synchrotron radiation in the presence of equipartition magnetic field is the major source of optical photons from the hot, optically-thin inner accretion flow during this hard state. We observed QPO like features at $\sim$18 mHz in the optical and X-ray power spectra with at

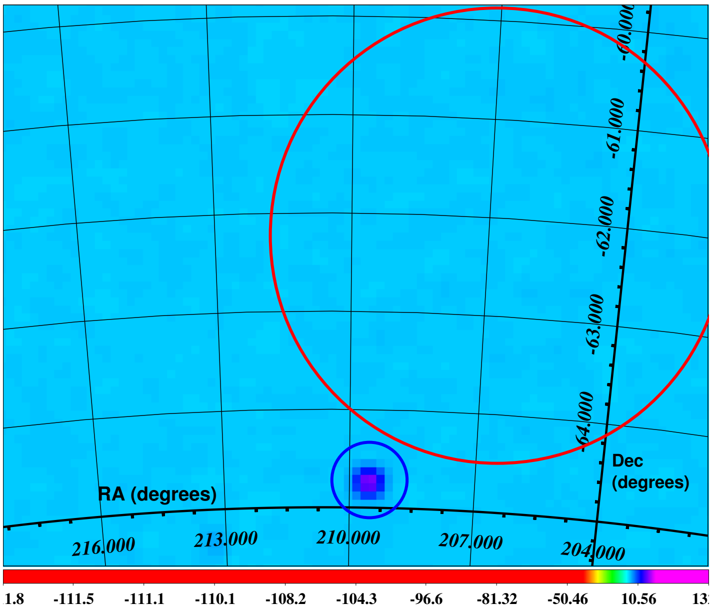

Figure 1. 22.0-60.0 keV *INTEGRAL*/IBIS hard X-ray image of GS 1354-64 (circled in blue) constructed by superimposing all pointings. In the hard X-ray band, the source is significantly detected. The position of the historical (Chodil et al. 1967) soft X-ray transient Cen X−2 is shown by the red circle, and given the uncertainties involved are consistent with being the same source in spite of their different spectral properties (see Kitamoto et al. (1990)).

least 99% confidence level. With an increase in the mass accretion rate, both QPOs disappear from the PDS and no correlation/anti-correlation between X-ray and optical variability are observed.

2 OBSERVATIONS

2.1 *SALT*/BVIT analysis

The optical observations of the source were taken on two nights – 05 July, 2015 and 08 August, 2015 under clear sky conditions using the Berkley Visible Imaging Tube (BVIT) mounted on the South African Large Telescope (SALT) (Welsh et al. 2012). BVIT is a micro-channel plate photon counting detector with an active geometric area of 25 mm^2 and capable of tagging individual events with a precision of 25 ns (Welsh et al. 2012; McPhate et al. 2012). Both observations of GS 1354-64 were taken with 10 ms integration time, and details are provided in Table 1. During both observations, a comparison star was chosen with brightness nearly equal to that of the source. The first observation on 05 July, 2015 was taken using white light with the neutral density (ND) set to 0.5, while the second observation was taken in R, and again ND set to 0.5. The 'star D' listed in Table 1 of Casares et al. (2009) is used as a comparison star as it is the brightest in R. BVIT data are reduced using the IDL BVIT data extraction pipeline (McPhate et al. 2012). Barycentric corrections to the BVIT lightcurve are performed using `tcor` tools available with the ULTRACAM data analysis package[1].

2.2 *SWIFT*/XRT analysis

SWIFT/XRT monitored the X-ray outburst of GS 1354-64 with an approximate cadence of 2 days. XRT provides simultaneous imaging and spectroscopy in the energy range 0.3−10.0 keV. To ensure pile-up free operations, all XRT observations were taken with Window Timing (WT) mode, and a time resolution of 17 msec. We follow standard procedures for extracting lightcurve, spectra and responses from XRT raw data. Because of poor calibration and efficiency, counts in channels 0-29 (< 0.3 keV) are ignored. All channels from 0.3-10.0 keV are binned such that a minimum of 30 counts per energy bin are available during spectral fitting. On 05 July, 2015 and 08 August, 2015 XRT observations were taken simultaneously with SALT and details are provided in Table 1. Barycentric corrections to XRT photon arrival times are performed using the relationship (*Swift*/XRT team private communication):

$$T_1 = (t - T_{START})/86400 \quad sec$$
$$t_{COR} = T_{OFFSET} + (C_0 + C_1 * T_1 + C_2 * T_1^2) \times 10^{-6} \quad sec \qquad (1)$$

where

t is the time of interest, T_{START} and T_{OFFSET} are start time and offset time of the observation under consideration, t_{COR} is the corrected photon arrival time and C_0, C_1 and C_2 are coefficients that can be obtained from the latest clock correction file `swclockcor20041120v111.fits` which was last updated on January, 2016 and available on the HEASARC caldb website[2]. Because of calibration uncertainties below 0.5 keV (Pahari et al. 2015) and poor signal-

[1] deneb.astro.warwick.ac.uk/phsaap/software/ultracam/html

[2] heasarc.gsfc.nasa.gov/FTP/caldb/data/swift/mis/bcf/clock

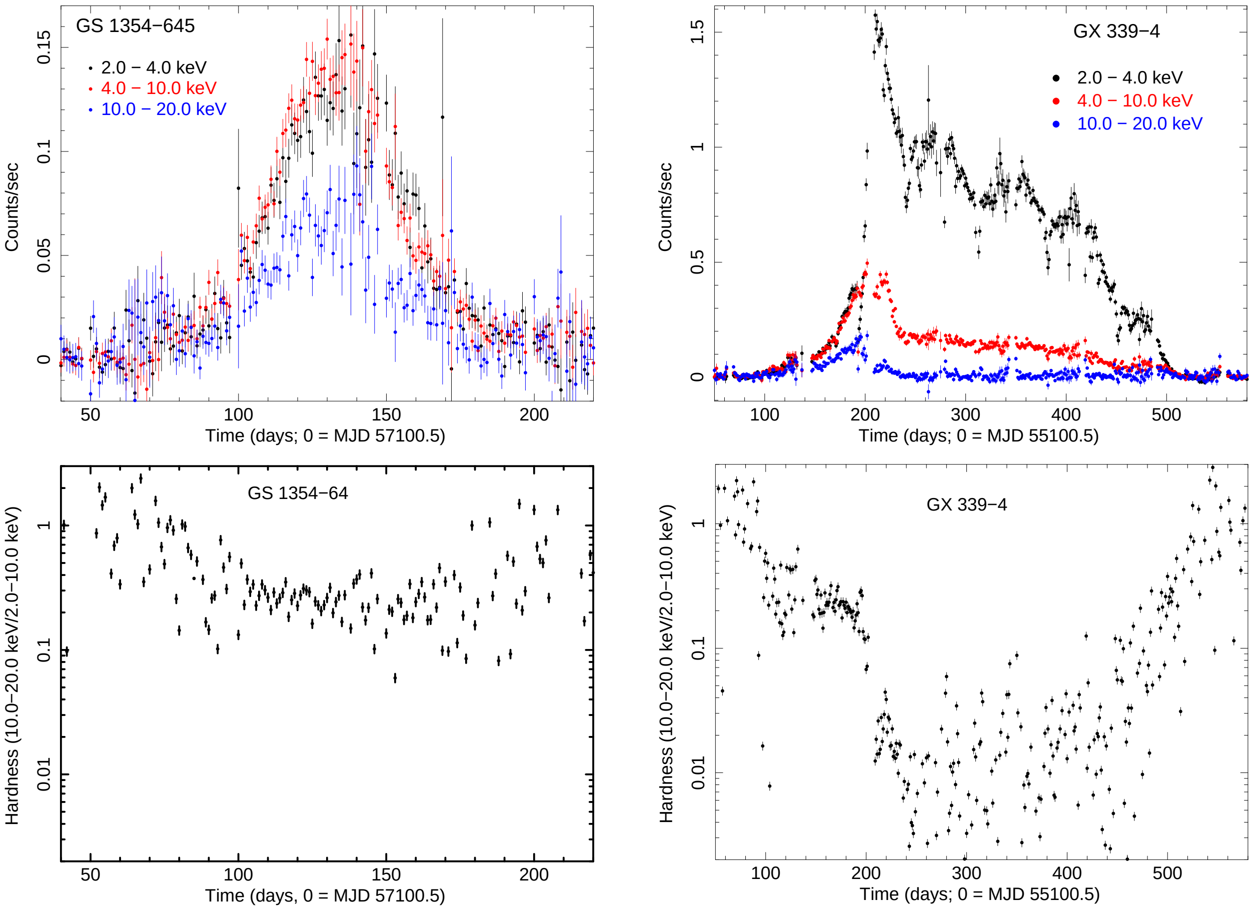

Figure 2. The top left panel shows one-day averaged *MAXI*/GSC lightcurves, obtained in energy bands - 2.0-4.0 keV (black), 4.0-10.0 keV (red) and 10.0-20.0 keV (blue) during the 2015 outburst of GS 1354-64. To compare the hard outburst from GS 1354-64 with a typical X-ray outburst from the canonical X-ray binary GX 339-4, the MAXI lightcurves of GX 339-4 for its 2010 outburst are plotted in the top right panel in energy bands similar to that of GS 1354-64. The hardness ratio, (10.0-20. keV/2.0-10.0 keV) is shown as a function of time in the bottom left and bottom right panels for both outbursts from GS 1354-64 and GX 339-4 respectively. The drop in hardness by ∼2-3 orders of magnitude at the peak in GX 339-4 is clearly visible compared to the small drop in hardness at the peak in GS 1354-64.

to-noise above 8 keV, we use the spectra in the energy range 0.5-8.0 keV for model fitting.

2.3 *INTEGRAL* analysis

INTEGRAL took 26 public pointing observations of GS 1354-64 between 05 July, 2015 UTC 00:54:33 and 05 July, 2015 UTC 22:11:34 during revolution no. 1560. The OMC, SPI, IBIS, JEMX1 and JEMX2 detectors of *INTEGRAL* were simultaneously on during each pointing. Observation details are provided in Table 1. All 26 archival data sets were processed and analysed using the INTEGRAL Offline Science Analysis (OSA; Goldwurm et al. (2003)) package v. 10.2, the `Instrument Characteristics v 10.2` and the `Reference Catalogue v. 40.0`. Following standard procedures, images are created by combining all science windows (each pointing lasts for 2-3 ks). Then they were cleaned and spectra extracted. In all four detectors - SPI, IBIS, JEM-X1 and JEM-X2 the source is detected with at least 6-sigma significance which does not change with energy. To generate JEM-X1 and JEM-X2 spectra and corresponding responses, energy bins with up to 16 channels are used so that maximum numbers of energy bins in 3.0-35.0 keV can be obtained. Since the low-energy threshold of IBIS/ISGRI onboard INTEGRAL has increased since launch, we ignore IBIS data below 22.0 keV. For SPI, we use the energy range of 25.0-1000.0 keV for spectral analysis.

2.4 Check for contamination

The position of GS 1354-64 in the sky is often confused with the brightest soft X-ray transient Cen X-2 due to large uncertainties in the latter X-ray location. During its 1967 outburst, Cen X-2 showed a soft X-ray flux ∼50 times higher than that observed from GS 1354-64 and the spectra showed variations in power law indices between 1.15 and 2.8 (Cooke & Pounds 1971; Francey 1971). On the other hand, GS 1354-64 is categorized as a hard X-ray transient which never reached the canonical high soft spectral states and state transitions. In Figure 1, a 22.0-60.0 keV *INTEGRAL*/IBIS cleaned image is shown combining all 26 exposures. This is the first hard X-ray image of GS 1354-64

Table 1. X-ray and optical observation details of GS 1354-64

Satellite/ Telescope	Instrument (mode)	Obs-ID	Date (dd-mm-yyyy)	Start time (hh:mm:ss)	Effective Exposure (sec)	average source count rate
Swift	XRT (WT)	00033811012	05-07-2015	18:30:28	965.1	14.9 ± 0.2
SALT	BVIT	20150705_BWCir	05-07-2015	18:18:11	2018.0	1013.6 ± 7.4
INTEGRAL	JEMX1	12700040001	05-07-2015	01:06:19	66260	10.3 ± 0.6
INTEGRAL	JEMX2	12700040001	05-07-2015	01:06:19	66160	10.4 ± 0.6
INTEGRAL	IBIS	12700040001	05-07-2015	01:06:19	52650	47.5 ± 0.2
INTEGRAL	SPI	12700040001	05-07-2015	01:06:19	53450	0.064 ± 0.003
Swift	XRT (WT)	00033811042	08-08-2015	18:09:30	507.5	28.7 ± 0.3
SALT	BVIT	20150808_BWCir	08-08-2015	17:47:42	2236.0	382.3 ± 4.6

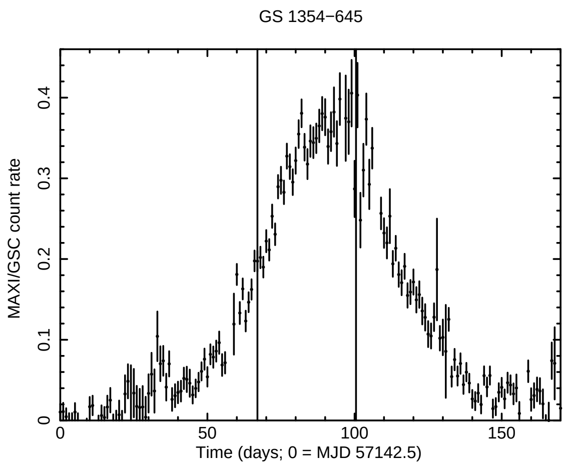

Figure 3. One day averaged *MAXI*/GSC lightcurve of GS 1354-64 during 2015 outburst in the energy range 2.0-20.0 keV. The times of two *SALT* observations simultaneous with *Swift* are marked as vertical lines.

observed with *INTEGRAL*. At the position of GS 1354-64, the source is detected with more than 10σ significance (shown in blue circle) whereas within the red circle of Cen X-2 (Chodil et al. 1967), no source is detected above the background limit. However, due to poor spatial resolution, the position uncertainties of the mean position of Cen X-2 are ± 2.5 degrees (Chodil et al. 1967). A possibility could still be that they are the same source (Kitamoto et al. 1990).

Using *Swift*/XRT photon counting (PC) mode data, we are also able to extract the source image in the 0.3-10.0 keV energy range. We obtain a highly significant detection ($> 20\ \sigma$), however due to strong, uncorrectable pile up, we cannot proceed further with PC mode data analysis.

3 RESULTS

3.1 Timing analysis and results

In order to understand the nature of the outburst, we compare the *MAXI* one-day averaged lightcurve of the entire 2015 outburst of GS 1354-64 with the recently observed outburst from a canonical BHXB GX 339-4. In the top panels of Figure 2, the *MAXI* lightcurve of GS 1354-64 (top left) and GX 339-4 (top right) are shown in three different energy bands. From both panels it may be noted that 2.0-4.0 keV peak count rate in GX 339-4 is $\sim$ 3 times higher than the peak count rate in 4.0-10.0 keV and $\sim$ 8 times higher than the peak count rate in 10.0-20.0 keV. This implies that soft band flux dominates hard band flux. On the other hand, 2.0-4.0 keV peak count rate in GS 1354-64 is similar to the peak count rate in 4.0-10.0 keV and $\sim$ 2 times higher than the peak count rate in 10.0-20.0 keV. This implies that hard band flux is more comparable to the soft band flux, a behaviour different to that observed in GX 339-4. The spectral state evolution during both outbursts from GS 1354-64 and GX 339-4 is shown as the hardness ratio (ratio of count rate in 10.0-20.0 keV and 2.0-10.0 keV) plot in the bottom panels of Figure 2. Transition from the hard to soft state is clearly observable in GX 339-4 as the hardness drops by $\sim$2-3 orders of magnitude at the peak count rate. But for GS 1354-64, the hardness ratio at the peak of outburst does not change dramatically beyond the hard state hardness level ($\sim$0.2). Therefore unlike GX 339-4, GS 1354-64 does not trace a canonical 'q' shape in the hardness intensity diagram of BHXBs. This is a typical characteristic of the hard outbursts which are rare compared to that observed from GX 339-4. It is not clearly understood what is the driving parameter that causes variation in the nature of X-ray outbursts from different X-ray binaries, e.g., hard X-ray outbursts in some BHXBs (e.g., GS 1354-64, SWIFT J1753.5-0127 (Shaw et al. 2016)), while canonical soft X-ray outbursts in the majority of sources (e.g., GX 339-4 (Miyakawa et al. 2008), XTE J1859+226 (Casella et al. 2004), XTE J1652-453 (Hiemstra et al. 2011) etc.) and a mix of hard and soft X-ray outbursts in a few other sources (e.g., H 1743-322 (Zhou et al. 2013) etc.).

The two observation times taken with *SALT* are shown using two vertical lines in Figure 3 where the 2.0-20.0 keV *MAXI* lightcurve of the entire 2015 outburst is shown. It may be noted that two observations were taken during two different X-ray fluxes - the first during the rising phase of the outburst on 05 July, 2015 (MJD 57209) and the second at peak of the X-ray outburst on 08 August, 2015 (MJD 57243). If we compare the present outburst (also from Figure 1 in Koljonen et al. (2016)) with the 1997 outburst from Brocksopp et al. (2001), the optical outburst peak occurs during the rising part of the X-ray outburst while a significant decline in the optical is observed during X-ray outburst peak. Therefore, changes in accretion parameters are expected between both observations taken simultaneously with *SALT* and *Swift*.

On 05 July, 2015, the strictly simultaneous data obtained with *SALT*/BVIT and *Swift* are shown in Figure 4 using 2.0 sec binning. The uncorrected, raw source lightcurve, the background-corrected comparison star and background & atmospheric variation corrected source lightcurve obtained from *SALT*/BVIT during the same observation are shown in panels A, B and C of Figure 4 respectively. The *Swift*/XRT lightcurve shows occasional short flares which are not seen in the *SALT*/BVIT data. Fast variability of the order of few tens of seconds as well as slow variability of the order of few hundreds of seconds are observed in the optical lightcurve (panel C in Figure 4). These long and short term variability components are absent in the comparison star lightcurve which implies that they are intrinsic to GS 1354-64. Both variability components on time-scales of few tens of milliseconds to hundreds of seconds are also observed in the optical lightcurve during the 2015 outburst of V404 Cyg (Gandhi et al. 2016; Kimura et al. 2016). A close inspection of simultaneous X-ray and optical lightcurves reveals a hint of lagged anti-correlation (e.g., forwarding the time axis of optical lightcurve by 0-20 sec, then short optical flares at ∼200 sec, ∼410 sec, ∼590 sec and ∼690 sec would correspond to dips in X-ray lightcurve at ∼205 sec, ∼420 sec, ∼610 sec and ∼710 sec respectively).

3.2 Power Density Spectra

To quantify variability, we compute power density spectra (PDS) of simultaneous X-rays (red) and optical (black) time-series on 05 July, 2015 shown in the left panel of Figure 5. Both PDS are rms normalized and Poisson noise subtracted. A quasi periodic oscillation (QPO) like feature at 18 ± 1.3 mHz is observed in both PDS. The fractional rms amplitude (in per cents) of X-ray and optical PDS are 23.8 ± 1.9 and 5.6 ± 1.7 respectively. We fit the PDS with two models : (1) power-law and (2) power-law + Lorentzian. For the optical, the change in χ^2 = - 19 for change of *dof* 3 when Lorentzian is included. An F-test between two models yields an F statistic value = 13.78 and the probability = 3.45×10^{-6}. In the case of the X-ray PDS, the change in χ^2 = -29 for change of *dof* 5. The F-test yields F statistic value = 7.5 and the probability = 7.15×10^{-5}. In order to compute the confidence level on the detection of QPOs from X-ray and optical time-series, we follow the recipe for testing the significance of peaks in the periodogram of red noise data provided by Vaughan (2005). If the red noise can be fitted by a powerlaw continuum, then low significance peaks can be rejected accurately using his recipe. Using the fitted the continuum PDS with powerlaw and computing confidence level, we find that the peak X-ray power in the PDS at the QPO frequency is higher than a 99.9% confidence level while the peak optical power in the source PDS at the position of QPO frequency touches the 99% confidence level.

Near simultaneous detection of X-ray and optical QPOs have been reported earlier (Hynes et al. 2003) but for the first time we observe strictly simultaneous potential QPO candidates from both X-rays and optical PDS. Assuming that the time-scales of physical processes that are responsible for optical and X-ray QPOs are related to the length scale of accretion disc, simultaneous QPO detection implies the emission in both bands arise at similar length scales. It may be noted that X-ray QPO at ∼ 18 mHz has been observed during the 1997 outburst of GS 1354-64 (Brocksopp et al. 2001).

3.3 X-ray/optical correlation study

To understand whether optical emission is the reprocessed X-ray from the outer accretion disc, we plot auto-correlation functions (which is cross correlation of a time-series with itself) of X-ray and optical time series in the right panel of Figure 5. In the order of 30 seconds, optical auto-correlation function is equally wide and have very similar pattern to that of X-ray auto-correlation function. Therefore, optical emission cannot be derived from the reprocessing of the X-ray at a time-scale < 30 sec. We perform X-ray/optical cross correlation (cross-correlation coefficient as a function of time-delay between X-rays and optical lightcurve) which is shown in the left panel of Figure 6. On the order of ten seconds, a strong anti-correlation is observed between X-rays and optical. A negative delay implies the X-ray band is delayed to the optical while anti-correlation implies out of phase variability between optical and X-ray. To compute the cross correlation, we use the tool `pydcf`[3] which is a python-based discrete cross correlation function which also works well with unevenly sampled data (Edelson & Krolik 1988; McHardy et al. 2014). We cross-checked our results with the `crosscor` tool available in `HEASOFT v. 6.19` and found that results from both tools match each other. The blue horizontal line in the left panel of Figure 6 marks the upper 99% confidence level for significance of the cross correlation function. For a two-tailed test, based on some simplified assumptions, the approximate 99% confidence interval (for which α = 0.01) is given by $\pm\, 2.58/\sqrt{N_s}$ where N_s is the sample size of the time-series (Chatfield 2004). Estimation of cross correlation coefficient outside the confidence interval is highly significant where the null hypothesis that the true cross correlation at a specified lag is zero must be rejected against the alternative hypothesis that the true coefficient is non-zero. We also compute the cross correlation between the optical and relatively soft (0.3-2.0 keV) & hard (2.0-8.0 keV) X-ray lightcurves from *Swift*/XRT separately, which are shown in the top and bottom right panels of Figure 6, respectively. The soft X-ray band shows relatively weak anti-correlation with optical while the hard X-ray shows very strong anti-correlation (more significant than 99.7% confidence level). This indicates that the region in accretion flow where optical photons are generated are strongly coupled to hard X-ray generating region than soft X-ray.

3.4 Checks on comparison star

To confirm that observed features are not due to any instrumental, atmosphere or background artifacts, we compute the optical PDS of the background-corrected comparison star in the same frequency range as the source. In the comparison star PDS, shown in the left panel of Figure 7, no QPO like features are observed with a confidence level higher than 90% and the integrated rms power in the optical PDS is about one order of magnitude less than the optical rms power of GS 1354-64. This implies that the QPO like feature

[3] `https://github.com/astronomerdamo/pydcf`

in the left panel of Figure 5 is due to the source only. We also check the cross correlation between the simultaneous optical lightcurve of the comparison star and X-ray lightcurve of GS 1354-64 and found no significant anti-correlation which is shown in the right panel of Figure 7. This implies that the lagged anti-correlation is due to the source.

3.5 X-ray high − optical low state

The second observation was taken on 08 August, 2015 when the X-ray outburst reached the peak intensity (as observed from Figure 3). The optical lightcurves obtained from *SALT*/BVIT are shown in the top three panels (panel A, B and C) of Figure 8 while the background-subtracted, simultaneous *Swift*/XRT lightcurve in the energy range 0.3-8.0 keV is shown in the bottom panel (panel D).

Comparing Figure 8 and Figure 4, we may note the existence of possible anti-correlated behaviour in the X-ray and optical fluxes on short time-scale during different observations. While the *Swift*/XRT count rate increases from ∼15 cts/sec to ∼29 cts/s, the optical count rate decreases. A significant decrease in optical flux on-short time scales can be observed in the source lightcurve in Figure 8 where the count rate decreases by a factor of ∼3 in ∼500 sec. A consistency check on this trend is possible using the light curve presented in Figure 1 of Koljonen et al. (2016). Interpolating between their data points to our dates of observation, implies a decrease in V band flux on both dates.

To determine the R magnitude during the second observation on 08 August 2015, we use SALTICAM images taken immediately after BVIT observation. We use the finding chart provided by Casares et al. (2009) including field stars for performing relative photometry. The comparison star in our observation is listed in Table 1 of Casares et al. (2009) as a nearby 'Star D' which has an R magnitude of 17.361. At the position of star D (R.A = 13:58:04.0 and Dec. = -64:44:02.0 (J2000)), the SALTICAM image shows the total count rate of 119938 cts/s within a circular region of 7 arcsec while at the position of GS 1354-64, the total count rate within 7 arcsec circle is 117454 cts/s. This gives an R magnitude of ∼17.384 for the optical counterpart of GS 1354-64 on 08 August 2015. This is very close to the R magnitude observed by Koljonen et al. (2016) when compared to their nearest observation on MJD 57245. The *Swift*/UVOT U filter flux densities from Figure 1 of Koljonen et al. (2016) are close to ∼0.055 mJy and ∼0.038 mJy during first and second observations respectively, consistent with the decrease in optical strength between two observations. Such optical/X-ray anti-correlated behaviour, although not widely studied, may be generic to the accretion process during hard X-ray outbursts. We also have studied the PDS of X-ray and optical time-series which are shown in the left panel of Figure 9. In the frequency range of 1 mHz to 100 mHz, no QPOs have been detected in both and PDS are dominated by red noise. In the right panel of Figure 9, cross correlation between simultaneous X-ray and optical is shown as a function of time-delay. No features significant upto 90% confidence are observed in the cross correlation pattern. Therefore, two important features − (1) simultaneous QPOs from optical and X-ray variability and (2) strong anti-correlation between X-ray and optical which are observed on 05 July 2015 are completely absent from X-ray and optical variability observed on 08 August 2015. This indicates that the increase in mass accretion rate from 05 July, 2015 to 08 August, 2015 causes QPOs to disappear. However, during both observations, the integrated fractional rms of the X-ray PDS is higher than that of the optical by the factors of ∼4-5.

3.6 Spectral analysis and results

To check spectral-timing correlated evolution of the source, we perform mean energy spectral analysis of simultaneous *Swift*/XRT and *INTEGRAL* in the energy range 0.5-1000.0 keV as observed on 05 July 2015. The aim of the joint spectral fitting is to understand the spectral nature of the underlying continuum during which optical and X-ray QPOs and the lagged anti-correlation are observed. Because of hard nature of the outburst, the X-ray emission is expected to be dominated by powerlaw-like component. Therefore, to fit the joint spectra, we use the NTHCOMP model in XSPEC which describes hot flow emission as thermal Comptonization of soft seed photons (Zdziarski et al. 1996). The broadband spectra can be fitted with this model (χ^2/dof = 317/285) above 2.0 keV. However, a strong residual below 2 keV is observed in the *Swift*/XRT spectrum which deteriorates the broadband fitting (0.5-1000.0 keV) to an unacceptable level (χ^2/dof = 559/420). To account for this, we include the disc blackbody emission model DISKBB in XSPEC which represents the emission from the cold accretion disc surrounding the hot flow. With the addition of DISKBB, the fit improves significantly (χ^2/dof = 463/418; change in χ^2 = -96). To account for Galactic neutral absorption, we use the TBABS model which is allowed to vary during fitting. Cross calibration constants are used between various detectors. The best fit model yields an observed inner disc temperature of 0.12 ± 0.04 keV and measured inner disc radius of 3000 ± 500 km assuming a source distance of 25 kpc and inclination of 70° respectively. Both values represent a cold disc truncated at a large radius (translated to ∼100 R_s assuming a black hole mass of 8.0 M⊙). The fitted `nthcomp` model component yields the photon power-law index of 1.48 ± 0.03 and Comptonizing, hot electron temperature of 90 ± 15 keV. These two parameters represent a hot inner flow with a very flat power-law like spectra. While fitting with the `nthcomp` model, we tied the Comptonization seed photon temperature to the inner disc temperature. The column density (N_H) is found to be 0.68 ± 0.08 $\times 10^{22} cm^{-2}$ which is consistent with predicted Galactic absorption column density at the direction of GS 1354-64. Figure 10 shows the simultaneously fitted spectra from *Swift*/XRT, *INTEGRAL*/JEMXs and *INTEGRAL*/ISGRI in the top panel and the residuals of the fitted spectra are shown in the bottom panel.

With the same best fit model, we fit the *Swift*/XRT spectra on 08 August, 2015 in the energy range 0.5-10.0 keV since no simultaneous observation from any other instrument was present. The best fit yields an observed inner disc temperature to be 0.49 ± 0.06 keV and apparent inner disc radius to be 1300 ± 400 km. The power-law photon index in `nthcomp` model is 1.65 ± 0.05. Taking these values as face value and comparing to those from July 05, we note that the cold, inner disc moves inward, resulting in a higher inner disc temperature and reducing the strength of the hot flow. This does not cause a state transition but is enough to weaken any QPO from X-ray and optical bands

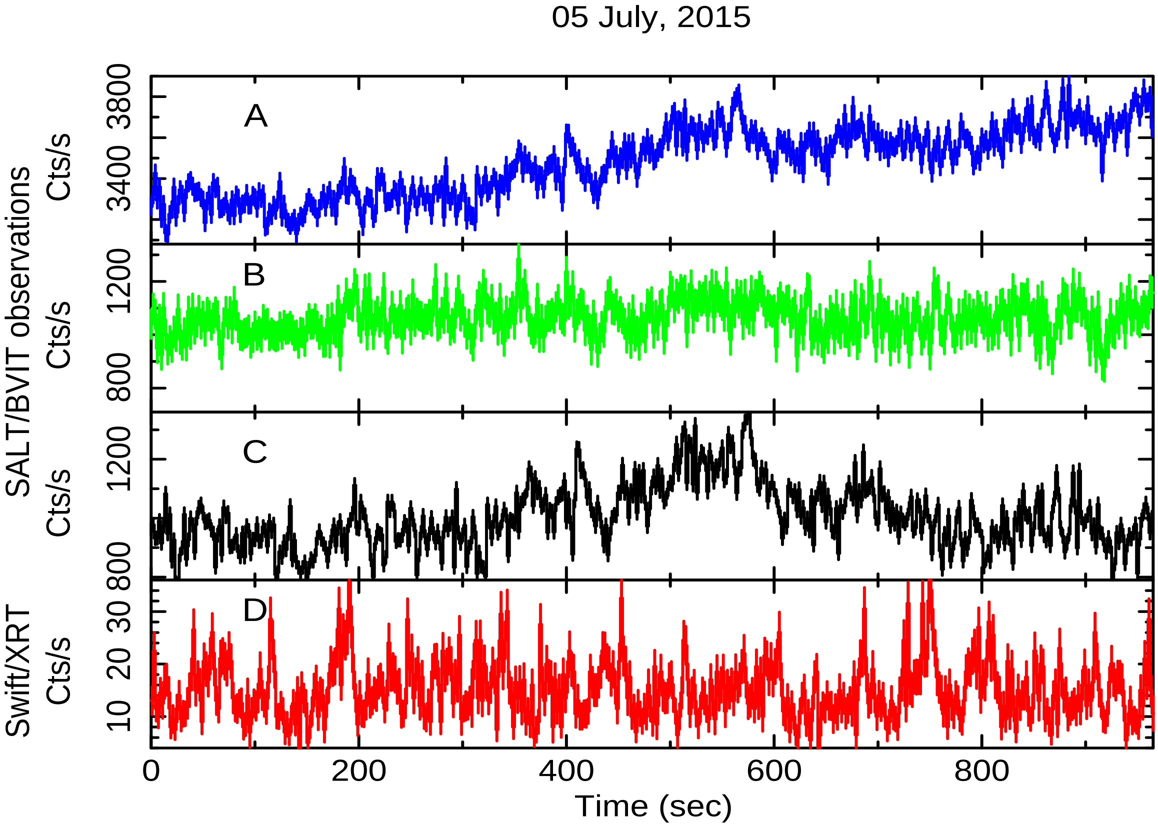

Figure 4. Strictly simultaneous lightcurves of GS 1354-64 as observed from *SALT*/BVIT and *Swift*/XRT on 05 July, 2015. Different panels show the raw, uncorrected *SALT*/BVIT optical lightcurve of GS 1354-64 (panel A), the background-corrected comparison star lightcurve (panel B), background & atmospheric variation corrected source lightcurve (panel C) and background subtracted X-ray lightcurve from *Swift*/XRT (panel D). For clarity, all lightcurves are binned to 2 sec time resolution.

below our detection limit. Consequently, the X-ray and optical that show opposite phases on 05 July, 2015, loose this phase correlation on 08 August, 2015 when the X-ray flux increases by a factor of ∼2.

4 DISCUSSION & CONCLUSION

Using simultaneous X-ray (*Swift*/XRT and *INTEGRAL*) and optical (*SALT*/BVIT) data on two occasions, we show that during the rising phase of the X-ray outburst in GS 1354-64, the luminous hard state corresponds to the optical high state. The drop in optical is also consistent with the U filter flux density from *Swift*/UVOT (Koljonen et al. 2016). A potential QPO is observed at ∼ 18 mHz in X-ray and optical PDS with at least 99% confidence level and a significant anti-correlation is found between optical?X-ray with optical photons leading X-ray photons. Best fit parameters from the broadband spectra in 0.5-1000.0 keV indicate the presence of a cold, truncated disc (∼ 0.12 keV) with hot, optically thin inner flow. The hot flow spectrum has a power-law photon index ∼1.48 and the electron temperature of ∼ 90 keV. Our energy spectral study shows that an optically thin hot electron corona can co-exists with the geometrically thin, cold disc and the matter from the disc may be evaporated to feed the corona (Meyer et al. 2000). Therefore depending on the mass flow rate, the accretion flow consists of a cool accretion disc which truncates at certain radius and evaporates into the inner hot coronal flow which fills up the inner part of the accretion flow (Meyer et al. 2000). Evidence of disc truncation is often observed in stellar mass black hole X-ray binaries as well as low luminosity AGN like M87 (Reynolds et al. 1996), M81, NGC 4579 (Dewangan et al. 2004) and may occur at variable radius ranging from 100 R_s (R_s is the Schwarzschild radius = $2GM/c^2$) (Gammie 1999; di Matteo et al. 1999) to 1000 R_s. With increasing mass accretion rate, inner edge of the cool disc usually moves in and the truncation radius decreases.

4.1 Estimation of cyclo-synchrotron luminosity

In order to confirm that results from the variability analysis are consistent with a cyclo-synchrotron origin of optical photons, we estimate the flux of self absorbed cyclotron expected in the optical using the following procedure (Takahara et al. 1981):

$$F_{\rm cyclotron} = \frac{2\pi m_*^3 \nu_c^3 k T_{\rm e}}{3c^2} \tag{2}$$

where ν_c is the cyclotron frequency of the emitted photons originating from the hot electron plasma and gyrating in the equipartition disc magnetic field B so that $\nu_c = eB/2\pi m_e$; where e and m_e are electron charge and electron

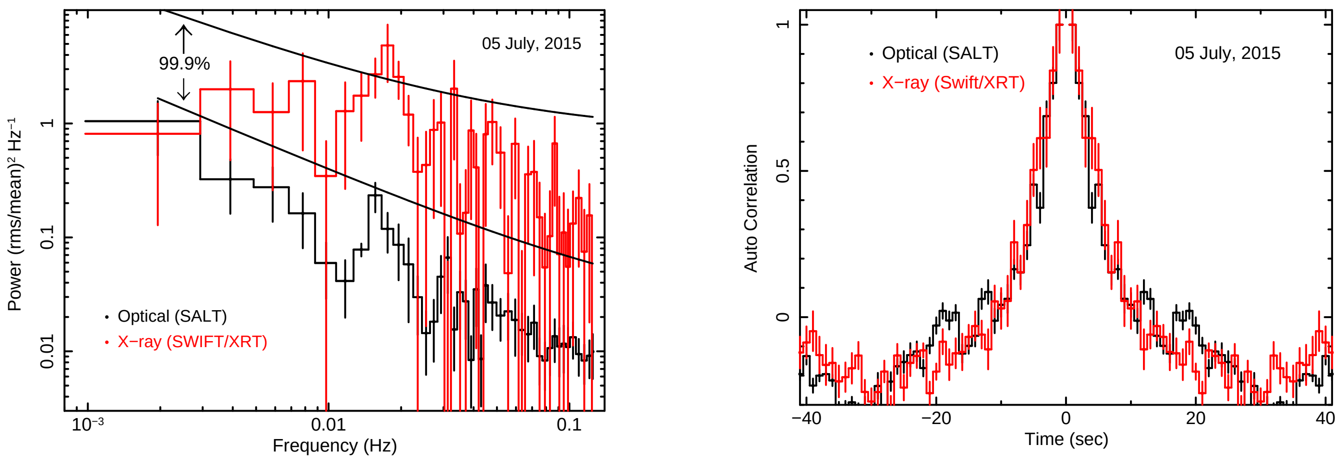

Figure 5. *Left panel*: Power density spectra (PDS) in the frequency range of 1 mHz to 100 mHz, obtained from simultaneous X-ray and optical time series as observed on 05 July, 2015 are shown in red and black respectively. Both PDS are rms normalized and white-noise subtracted. QPO like features at $\sim$ 18 mHz are observed in both PDS with at least 99% confidence. 99.9% confidence levels are shown by black lines. Auto-correlation function (ACF) of the X-ray (red) and optical (black) time series as observed on 05 July, 2015 are plotted in the right panel. Both auto-correlation functions have similar width at least upto 30 sec which is an evidence against reprocessing from X-ray to optical.

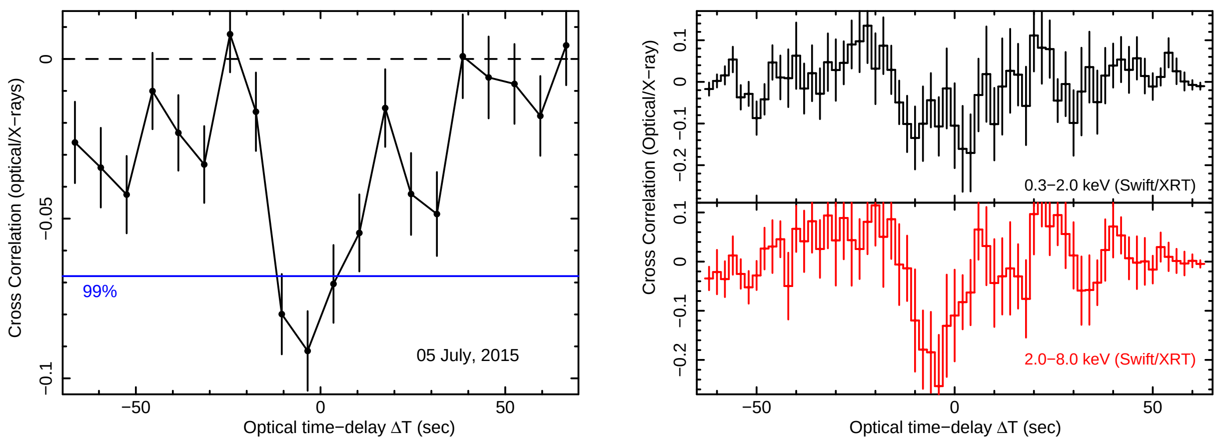

Figure 6. Left panel shows the plot of cross correlation function (CCF) as a function of time delays between simultaneous X-rays (0.3-8.0 keV) and optical time series as observed on 05 July, 2015. There is a strong anti-correlation observed between X-ray and optical lightcurves and the optical time series is delayed with respect to X-ray by $\leqslant$ 10 sec. The blue horizontal line shows the 99% confidence level of non-zero cross correlation coefficient. X-ray Energy dependence of the CCF is shown on the right panel where the CCF is constructed between optical and soft X-ray energy bands (0.3-2.0 keV; top right panel) and between optical and hard X-ray energy bands (2.0-8.0 keV; bottom right panel). Stronger anti-correlation is observed with the hard X-ray energy band than the soft X-ray energy bands.

rest mass respectively. Equipartition magnetic field at the inner disc for a moderately rotating black hole is estimated to be $\sim 10^7$ Gauss assuming turbulent viscosity in the disc is comparable to the magnetic viscosity. Shakura and Sunyaev (1973) estimated the inner disc magnetic field to be 2×10^7 Gauss. The recent accretion disc MHD simulation shows that the magnetic field due to MRI turbulences is of the order of 10^6 Gauss which is required for magnetic jet power (Tchekhovskoy et al. (2011) and references therein). However, the field strength of the disc magnetic field in the presence of hot flow is not well estimated. Assuming mass flow from the disc to the corona is comparable at the truncation radius, Meyer & Meyer-Hofmeister (2002) shows that $B^2_{\rm corona}/8\pi \approx 10^{-1.2}\ B^2_{\rm disk}/8\pi$. Assuming $B_{\rm disk} \sim 5 \times 10^6$ Gauss, we obtain $B_{\rm corona} \sim 3.16 \times 10^6$ Gauss. Using this magnetic field, the cyclotron frequency we obtain $\nu_c = 4.6 \times 10^{12}$ Hz which corresponds to the emission in Far Infrared band. However, cyclotron emission is highly absorbed up to many higher order harmonics. For the cyclotron emission to appear in the optical, i.e., $\nu = 4.8 \times 10^{14}$ Hz, ν/ν_c would be of the order of $\sim$ 104. Using numerical approach, it is shown that at $\nu/\nu_c \sim 100$, the harmonic order of the cyclotron emission (m_*) would be $\sim$ 300 when $kT_e/m_ec^2 \sim 0.25$ (Takahara et al. 1981; Takahara & Tsuruta 1982). With the decrease in electron temperature, lower order harmonics appear at similar emission coefficient. Therefore, we assume m_* to be 250 since the model fitted electron temperature is $\sim$ 100 keV (i.e., $kT_e/m_ec^2 \sim 0.2$). To compute

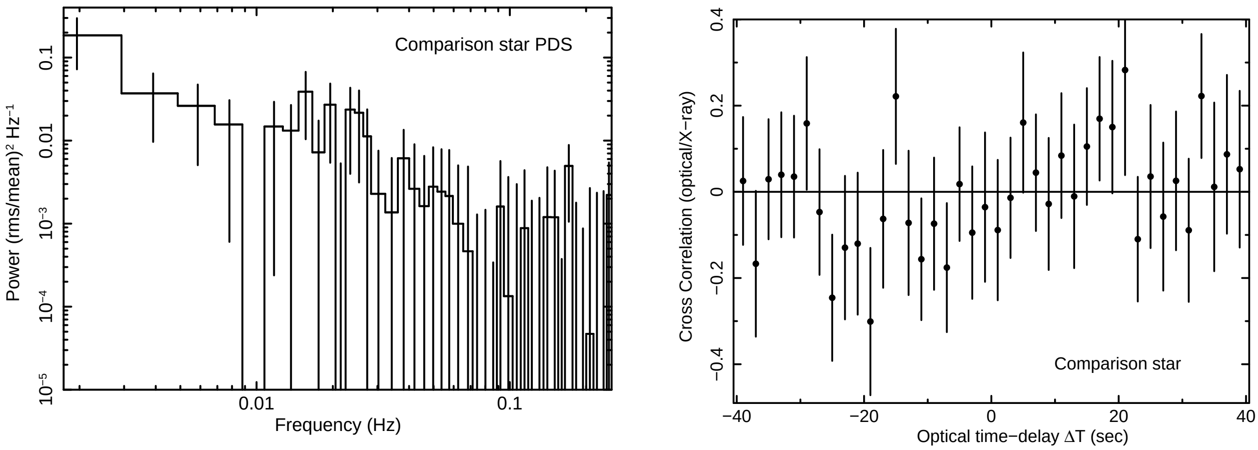

Figure 7. The left panel shows the optical power density spectrum (PDS) of the comparison star in the frequency range 1 mHz to 100 mHz where no QPO like feature is observed. The right panel shows the plot of cross correlation function (CCF) as a function of time delays between simultaneous X-rays time-series (0.3-8.0 keV) of the source GS 1354-64 and the optical time series of the comparison star as observed on 05 July, 2015. There is no significant anti-correlation observed between both lightcurves at any delay time confirming the anti-correlated lag observed in Figure 6 is due to the source only.

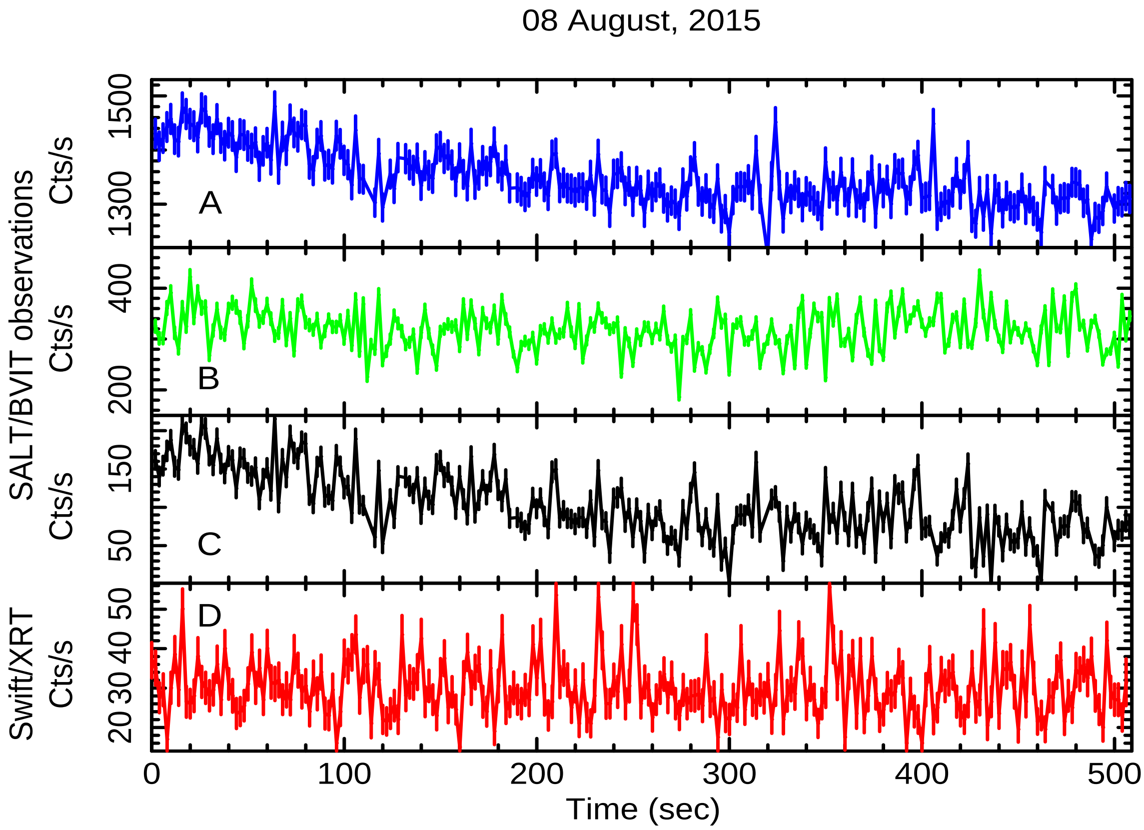

Figure 8. Strictly simultaneous lightcurves of GS 1354-64 as observed from *SALT*/BVIT and *Swift*/XRT on 08 August, 2015. Different panels show the raw, uncorrected *SALT*/BVIT optical lightcurve of GS 1354-64 (panel A), the background-corrected comparison star lightcurve (panel B), background & atmospheric variation corrected source lightcurve (panel C) and background subtracted X-ray lightcurve from *Swift*/XRT (panel D). For clarity, all lightcurves are binned to 2 sec time resolution.

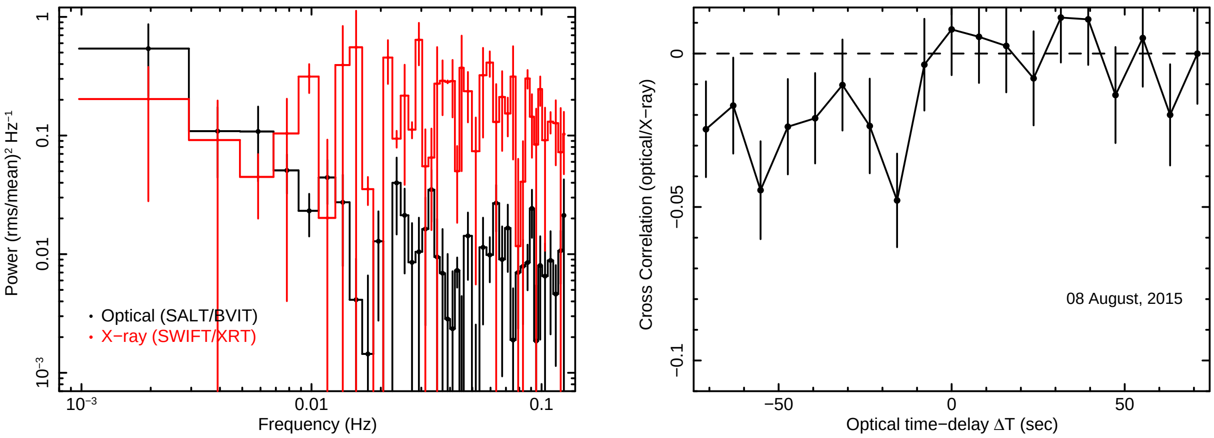

Figure 9. *Left panel :* Power density spectra (PDS) in the frequency range of 1 mHz to 100 mHz, obtained from simultaneous X-ray and optical time series as observed on 08 August, 2015 are shown in red and black respectively. Both PDS are rms normalized and whit-noise subtracted. *Right panel:* Plot of cross correlation function (CCF) as a function of time delays between simultaneous X-rays (0.3-8.0 keV) and optical time series as observed on 08 August, 2015 is shown. No significant anti-correlation or time delay is observed in the CCF.

self-absorbed cyclotron flux (which we assume to be manifested as the optical flux at higher order harmonics) $F_{\rm opt}$, we use the following relationship:

$$F_{\rm cyclotron} = F_{\rm opt} \simeq 4 \times 10^4 \times (kT_{\rm e}/m_{\rm e}c^2) \times m_*^3 \times (B_{\rm corona}/10^4{\rm Gauss})^3 \text{ ergs s}^{-1} \text{ cm}^{-2} \quad (3)$$

Using earlier estimations of B_{corona}, kT_e/m_ec^2 and m_* in equation 3, we obtain $F_{opt} \sim 2.48 \times 10^{17}$ ergs/s/cm^2. From the joint fitting of *Swift* and *INTEGRAL* X-ray spectra in the energy range 0.5−1000.0 keV, inner disc radius is found to be 2900 ± 600 km (calculated from the normalization of `disbb` and `ezdiskbb` model assuming colour correction factor of 1.7). If we assume the mass of the black hole to be 8.0 M$\odot$, then this radius is translated to be ∼ 100-130 R_s (R_s = Schwarzschild radius). If we assume that the inner part is filled with hot flow upto 100 R_s, then the optical luminosity would be $L_{opt} \simeq 3.31 \times 10^{35}$ ergs/s. From the Figure 1 of Koljonen et al. (2016), if we consider SMARTS Bessel R magnitude of GS 1354-64 to be ∼17.18 on 05 July, 2015, corresponding optical flux will be ∼2.7× 10^{-12} ergs/s/cm^2. For an approximate distance of ∼30 kpc, the optical luminosity would be ∼3 × 10^{35} ergs/s which is very close to our estimation from theoretical considerations as well as fitted spectral parameters. From the *Swift*/XRT and *INTEGRAL* joint spectral fitting, 0.1−1000.0 keV unabsorbed X-ray flux is found to be 1.69 × 10^{-8} ergs/s/cm^2. If we assume the distance to the source to be 30 kpc, the X-ray luminosity would be $L_{x-ray} \simeq 13.82 \times 10^{37}$ ergs/s. Therefore, $L_{opt}/L_{x-ray} \simeq$ 0.24%. Therefore, the origin of optical photons is highly consistent with cyclo-synchrotron process.

4.2 Comparison with 1997 outburst

During the 1997 hard state outburst of GS 1354-64 (Brocksopp et al. 2001), the B, R and V band fluxes are high during the rising phase of the X-ray outburst (from Figure 1 of Brocksopp et al. (2001)) and drop significantly at the peak of the outburst. Interestingly, this also matches with two optical observations taken by SALT and simultaneously taken by *Swift*/UVOT (Koljonen et al. 2016) during the latest outburst. Not only that, X-ray lightcurve profile of the current outburst also matches with that during 1997 (Figure 1 Brocksopp et al. (2001)). This indicate that the accretion mechanism during different hard X-ray outbursts in GS 1354-64 is very similar. It is also clear that Radio jets are observed during the rising phase of the X-ray outbursts and the Radio luminosity falls rapidly afterwards. If we assume that 1997 and 2015 outbursts in this source follow similar accretion-ejection mechanism, then we expect strong jet activity during our first optical observation. Therefore, the formation of jet base (probably a large spherical corona) which may provide strong non-thermal Comptonization of seed photons (either optical/UV photons generated inside hot flow or photon from the cold disc surrounding the hot inner flow) is possible during our simultaneous *Swift*, *SALT* and *INTEGRAL* observations. An evidence for such jet-base/corona formation may comes from the very flat power-law index (∼ 1.48) and very hot coronal temperature (∼ 100 keV) obtained from joint *Swift* and *INTEGRAL* spectral fitting.

The spectral state during simultaneous *Swift*, *SALT* and *INTEGRAL* observations can be described as the luminous hard state (Yuan & Zdziarski 2004) in which the nature of accretion is not well-understood. Assuming the compact object mass of GS 1354-64 to be 8 M$\odot$, the Eddington luminosity would be 10.1 × 10^{38} ergs/s. Therefore, the observed X-ray luminosity, obtained from spectral fitting is ∼ 14% of the Eddington luminosity. On the other hand, during the canonical low hard state, the X−ray luminosity is usually < 1% of the Eddington luminosity. Therefore, the current observation is more luminous than typical low hard state, at least by an order of magnitude.

4.3 On the origin of X-ray/optical QPOs

The ∼ 55 sec QPOs observed from optical and X-ray lightcurves are expected from the variation in the size of the hot inner flow. In the present work, if we assume the

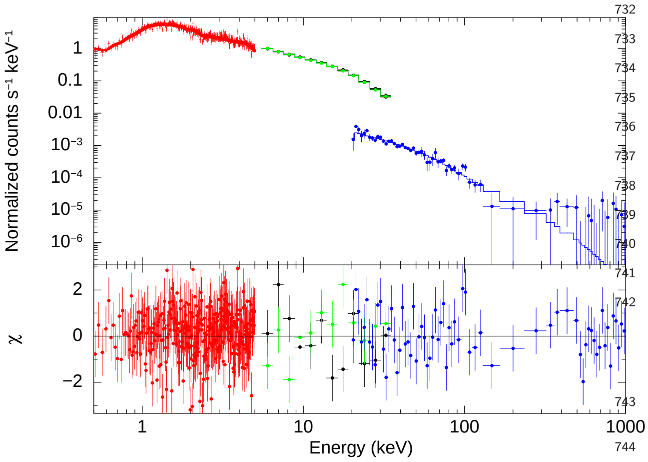

Figure 10. Joint spectral fitting with simultaneous spectra obtained from *Swift*/XRT (red), *INTEGRAL*/JEMX1 (green), *INTEGRAL*/JEMX2 (black) and *INTEGRAL*/ISGRI (blue) on 05 July, 2015 are shown in the top panel. For spectral modelling, disc blackbody `diskbb` and thermal comptonization models `nthcomp` are used. The bottom panel shows the residual of the fitting.

size of the hot inner flow is same as the disc truncation radius which is $\sim$ 3000 km, then following the argument of Fabian et al. (1982), the in-fall time-scale can be calculated as high as 50-60 sec depending upon the hot flow filling factor which could be less than 1. It is interesting to note that excess in the optical and X-ray power density spectra at the similar frequencies ($\sim$ 8 mHz) has also been reported by Veledina et al. (2015) in SWIFT J1753.5−0127 and they interpreted the simultaneous X-ray and optical excess as the Lense−Thirring precession of the inner hot flow (Stella & Vietri 1998; Ingram, Done & Fragile 2009). Precession of hot, inner flow may play an important role here for two reasons : (1) we observe X-ray and optical simultaneous QPOs at the time-scale of $\sim$ 55 sec during bright hard state. If optical QPO originates within the hot-flow by the means of the cyclo-synchrotron process and the observed QPO time-scale is same as the precession time-scale then precession is a natural explanation of observed QPOs. (2) Hard X-ray variabilities are found to have stronger anti-correlated with the optical variabilities than soft X-ray. This implies that soft photons may not participate in the process that causes anti-correlation between X-ray and optical. Therefore, the origin of the soft photon could be the truncated, cold outer disc, rather than some mechanism associated with the precessing hot flow. This is also supported by the fact that no significant excess is detected in the PDS of soft X-ray lightcurve (0.3-2.0 keV) from *Swift*/XRT. However in an alternate scenario, weakening of anti-correlation in softer X-ray band has been explained by the cyclo-synchrotron self-Compton-disc reprocessing model by Veledina, Poutanen & Vurm (2011). During the second optical observation while the X-ray burst reaches the peak intensity, QPOs from both X-ray and optical band disappeared from the PDS and the inner disc temperature increase by a factor of $\sim$ 4. Therefore, the enhanced inner disc activity as it moves inward due to increased mass accretion rate may inject instabilities that weaken such hot flow precession. Disruption of hot flow can be caused by radiation pressure instability since the luminosity at the peak of the X-ray outburst reached $\sim$ 40% of the Eddington luminosity. Exploring the origin of QPOs further is currently out of scope of the present work.

Missions like ASTROSAT which have optical/UV and X-ray detectors with the capability of event recording with high time resolution will be able to measure optical and X-ray variability simultaneously from different BHXBs. This would be immensely important for deeper understanding of accretion mechanism during luminous hard state.

ACKNOWLEDGEMENTS

MP acknowledge that a major part of this work is done under UGC-UKIERI thematic partnership grant UGC 2014-15/02 at the School of Physics & Astronomy, University of Southampton, UK. MP is thankful to the SWIFT and INTEGRAL team members for arranging X-ray observations simultaneous to the SALT telescope observation on short notice. BVIT observations were obtained with the Southern African Large Telescope (SALT) under program 2014-1-MLT-003 (PI: M.M. Kotze). MP also thanks SAAO team for making multiple efforts for the observation due to bad weather. PG acknowledges funding from STFC (ST/J003697/2) and thanks T. Marsh for the software. This research has made use of data obtained through the High Energy Astrophysics Science Archive Research Center online service, provided by the NASA/Goddard Space Flight Center.

REFERENCES

Apparao, K. M. V. 1984, A&A, 139, 375
Brocksopp, C., Jonker, P. G., Fender, R. P., Groot, P. J., van der Klis, M., Tingay, S. J. 2001, MNRAS, 323, 517
Casares, J., Orosz, J. A., Zurita, C., Shahbaz, T., Corral-Santana, J. M., McClintock, J. E. et al. 2009, ApJS, 181, 238
Casares, J., Zurita, C., Shahbaz, T., Charles, P. A., Fender, R. P. 2004, ApJ, 613, L133
Casella, P., Belloni, T., Homan, J., Stella, L. 2004, A&A, 426, 587
Chatfield, C., 2004, *The Analysis of Time series, An Introduction*, sixth edition. Chapman & Hall/CRC, New York. 333 pp.
Chodil, G.; Mark, Hans; Rodrigues, R.; Seward, F.; Swift, C. D. et al. 1967, PhRvL, 19, 681
Cooke, B. A., Pounds, K. A. 1971, Nature Phys. Sci., 229, 144
Coriat, M., Tzioumis, T., Corbel, S., Fender, R., Miller-Jones, J. 2015, Astronomer Telegram 7656
Corral-Santana, J., Munoz-Darias, T., Carballo-Bello, J. A., Bauer, F. E. 2015, Astronomer Telegram 7620
Dewangan, G. C., Griffiths, R. E., Di Matteo, T., Schurch, N. J. 2004, ApJ, 607, 788
de Jong, J. A., van Paradijs, J., Augusteijn, T. 1996, A&A, 314, 484
di Matteo, T., Celotti, A., Fabian, A. C. 1999, MNRAS, 304, 809
Durant, M., Shahbaz, T., Gandhi, P., Cornelisse, R. et al. 2011, MNRAS, 410, 2329
Durant, M., Gandhi, P., Shahbaz, T., Peralta, H. H., Dhillon, V. S. 2009, MNRAS, 392, 309
Durant, M., Gandhi, P., Shahbaz, T., Fabian, A. P. et al. 2008, ApJ, 682, L45

Edelson, R. A. & Krolik, J. H. 1988, ApJ, 333, 646
Esin, A. A., Kuulkers, E., McClintock, J. E., Narayan, R. 2000, ApJ, 532, 1069
Esin, A. A., McClintock, J. E., Narayan, R. 1997, ApJ, 489, 865
Fabian, A. C., Guilbert, P. W., Motch, C. et al. 1982, A&A, 111, L9
Francey, R. J. 1971, Nature Phys. Sci., 229, 228
Gammie, C. F. 1999, ApJ, 522, L57
Gandhi, P., Littlefair, S. P., Hardy, L. K., Dhillon, V. S., Marsh, T. R., Shaw, A. W. et al. 2016, MNRAS, 459, 554
Gandhi, P., 2009, ApJ, 697, L167
Gandhi, P. et al., 2010, MNRAS, 407, 2166
Gandhi, P. et al., 2008, MNRAS, 390, L29
Goldwurm, A., David, P., Foschini, L., Gros, A., Laurent, P. et al. 2003, A&A, 411, L223
Hiemstra, B., Meńdez, M., Done, C., Diáz, T. M., Altamirano, D., Casella, P. 2011, MNRAS, 411, 137
Hynes, R. I., Haswell, C. A., Cui, W., Shrader, C. R. et al. 2003, MNRAS, 345, 292
Ingram, A., Done, C., Fragile, P. C. 2009, MNRAS, 397, L101
Kanbach G., Straubmeier C., Spruit H. C., Belloni T., 2001, Nature, 414, 180
Kimura, M., Isogai, K., Kato, T., Ueda, Y., Nakahira, S., Shidatsu, M., Enoto, T. et al. 2016, Nature, 529, 54
Kitamoto, S., Tsunemi, H., Pedersen, H., Ilovaisky, S. A., van der Klis, M. 1990, ApJ, 361, 590
Koljonen, K. I. I., Russell, D. M., Corral-Santana, J. M., Armas Padilla, M. et al. 2016, MNRAS, 460, 942
Makino, F. et al., 1987, IAU Circular no. 4342.
Malzac, J., Merloni, A. & Fabian, A. C. 2004, MNRAS, 351, 253
Malzac, J., Belloni, T., Spruit, H. C., Kanbach, G. 2003, A&A, 407, 335
McHardy, I. M., Cameron, D. T., Dwelly, T., Connolly, S., Lira, P., et al. 2014, MNRAS, 444, 1469
McPhate, J. B., Siegmund, O. H. W., Welsh, B. Y. et al. 2012, PhPro., 37, 1453
Merloni, A., Di Matteo, T., & Fabian, A. C. 2000, MNRAS 318, L15
Miller, J. M., Reynolds, M. T., Kennea, J., 2015, Astronomer Telegram 7614
Miller, J. M., Reynolds, M. T., Kennea, J., 2015, Astronomer Telegram 7612
Miyakawa, T., Yamaoka, K., Homan, J., Saito, K., Dotani, T., Yoshida, A., Inoue, H. 2008, PASJ, 60, 637
Motch, C. et al. 1983, A&A, 119, 171
Motch, C. et al. 1982, A&A, 109, L1
Meyer, F., Liu, B. F., Meyer-Hofmeister, E. 2000, A&A, 361, 175
Meyer, F., Meyer-Hofmeister, E. 2002, A&A, 392, 5
Pahari, M., Misra, R., Dewangan, G. C., Pawar, P. 2015, ApJ, 814, 158
Reynolds, C. S., Di Matteo, T., Fabian, A. C., Hwang, U., Canizares, C. R. 1996, MNRAS, 283, L111
Remillard, R. A., McClintock, J. E. 2006, ARA&A, 44, 49
Russell, D. M. & Lewis, F. 2015, Astronomer Telegram 7637
Russell, D. M. & Lewis, F. 2010, arXiv:1001.1244
Shahbaz, T., Linares, M., Nevado, S. P., Rodriǵuez-Gil, P., Casares, J., Dhillon, V. S., Marsh, T. R., Littlefair, S., Leckngam, A., Poshyachinda, S. 2015, MNRAS, 453, 3461
Shakura, N. I. & Sunyaev, R. A. 1976, MNRAS, 175, 613
Shakura, N. I. & Sunyaev, R. A. 1973, A&A, 24, 337
Shapiro, S. L., Lightman, A. P., Eardley, D. M. 1976, A&A, 204, 187
Shaw, A. W., Gandhi, P., Altamirano, D., Uttley, P. et al. 2016, MNRAS, 458, 1636
Stella, L., Vietri, M. 1998, ApJ, 492, L59
Takahara, F., Tsuruta, S., Ichimaru, S. 1981, ApJ, 251, 26
Takahara, F., Tsuruta, S. 1982, Prog. Theor. Phys., 67, 485
Tchekhovskoy, A., Narayan, R., McKinney, J.C. 2011, MNRAS, 418, L79
Uttley, P., Casella, P. 2014, SSRv, 183, 453
Uttley, P., McHardy, I. M., Vaughan, S. 2005, MNRAS, 359, 345
van Paradijs, J. & McClintock, J. E. 1994, A&A, 290, 133
Vaughan, S. 2005, A&A, 431, 391
Veledina, A., Revnivtsev, M. G., Durant, M., Gandhi, P., Poutanen, J. 2015, MNRAS, 454, 2855
Veledina, A., Poutanen, J., Vurm, I. 2011, ApJ, 737, L17
Welsh, B., Anderson, D., McPhate, J., Vallerga, J., Siegmund, O. H. W., Buckley, D., Gulbis, A., Kotze, M., Potter, S. 2012, IAUS, 285,99
Yuan, F. & Narayan, R. 2014, ARA&A, 52, 529
Yuan, F. & Zdziarski, A. A. 2004, MNRAS, 354, 953
Zdziarski, A. A., Johnson, W. N., Magdziarz, P. 1996, MNRAS, 283, 193
Zhou, J. N., Liu, Q. Z., Chen, Y. P., Li, J., Qu, J. L., Zhang, S., Gao, H. Q., Zhang, Z. 2013, MNRAS, 431, 2285

This paper has been typeset from a TEX/LATEX file prepared by the author.